Title:

T cells limit accumulation of aggregate pathology following intrastriatal injection of α-synuclein fibrils

Authors:

Sonia George[1], Trevor Tyson[1], Nolwen L. Rey[1, 2], Rachael Sheridan[3], Wouter Peelaerts[1], Katelyn Becker[1], Emily Schulz[1], Lindsay Meyerdirk[1], Amanda R. Burmeister[1], Jennifer A. Steiner[1], Martha L. Escobar Galvis[1], Jiyan Ma[1], Lena Brundin[1], and Patrik Brundin[1]

Sonia George: sonia.george@vai.org
Trevor Tyson: trevor.tyson@vai.org
Nolwen L. Rey: Nolwen.Rey@cnrs.fr
Rachael Sheridan: rachael.sheridan@vai.org
Wouter Peelaerts: wouter.peerlaerts@vai.org
Katelyn Becker: katelyn.becker@vai.org
Emily Schulz: emily.schulz@vai.org
Lindsay Meyerdirk: lindsay.meyerdirk@vai.org
Amanda Burmeister: Amanda.Burmeister@vai.org
Jennifer A. Steiner: jennifer.steiner@vai.org
Martha L. Escobar Galvis: martha.escobar@vai.org
Jiyan Ma: jiyan.ma@vai.org
Lena Brundin: lena.brundin@vai.org
Patrik Brundin: patrik.brundin@vai.org

Author Affiliation:

[1-] Center for Neurodegenerative Science, Van Andel Research Institute, Grand Rapids, Michigan, USA
[2-] Laboratory of Neurodegenerative Diseases, Institut François Jacob, MIRCen, CEA, CNRS, 92265 Fontenay-aux-Roses, France.
[3-] Flow Cytometry Core Facility, Van Andel Research Institute, Grand Rapids, Michigan, USA

Corresponding Author:

Sonia George
Center for Neurodegenerative Science
Van Andel Research Institute
333 Bostwick Ave., N.E.

Grand Rapids, Michigan 49503 USA

Email: sonia.george@vai.org

Phone: +1 616 234 5000

Abstract

α-Synuclein (α-syn) is the predominant protein in Lewy-body inclusions, which are pathological hallmarks of α-synucleinopathies, such as Parkinson's disease (PD) and multiple system atrophy (MSA). Other hallmarks include activation of microglia, elevation of pro-inflammatory cytokines, as well as the activation of T and B cells. These immune changes point towards a dysregulation of both the innate and the adaptive immune system. T cells have been shown to recognize epitopes derived from α-syn and altered populations of T cells have been found in PD and MSA patients, providing evidence that these cells can be key to the pathogenesis of the disease. To study the role of the adaptive immune system with respect to α-syn pathology, we injected human α-syn preformed fibrils (PFFs) into the striatum of immunocompromised mice (NSG) and assessed accumulation of phosphorylated α-syn pathology as well as microgliosis. Compared to wildtype mice, NSG mice had an 8-fold increase in phosphorylated α-syn pathology in the substantia nigra. We also reconstituted T and B cell populations in the NSG mice with cells isolated from a wildtype mouse spleen. Interestingly, reconstituting the T cell population decreased the accumulation of α-syn pathology and resulted in persistent microgliosis when compared to non-transplanted mice; reconstitution of B cells did not alter the nigral neuropathology. Our work provides experimental evidence that T cells play a role in the pathogenesis of α-synucleinopathies.

Keywords:

Parkinson's disease, multiple system atrophy, alpha-synuclein, phosphorylated alpha-synuclein, T lymphocytes, microglia

INTRODUCTION

The pathogenesis of Parkinson's disease (PD) and multiple system atrophy (MSA) are poorly understood, but neuroinflammation and α-synuclein (α-syn) aggregation are believed to play key roles [1-4]. Progressive spread of Lewy pathology is thought to contribute to clinical decline in PD and to be the result of cell-to-cell propagation of α-syn aggregates [5]. Neuroinflammation is believed to be involved in the initial formation and spread of α-syn aggregates [6-8]. Studies on postmortem tissue indicate that microglia are activated in PD [9-12] and in MSA [4]. Neuroinflammatory markers in the central nervous system of MSA patients are also observed [4,13-15]. Single nucleotide polymorphisms close to numerous immune system-related genes affect PD risk, further supporting a role for neuroinflammation in PD [16]. While the majority of studies exploring inflammation in PD have implicated changes in the innate immune system [17,18], the role of the adaptive immune system in PD has been explored to a lesser extent. Notably, peripheral immune cells enter the brain during neurodegeneration [19]. T lymphocytes are altered and infiltrate the brain in PD [20-27] and it has been reported that autoreactive T lymphocytes directed against α-syn are present in PD patients [28]. In PD models, T cell function has been linked to α-syn pathobiology [29-31] and to the death of dopamine neurons [8,32]. Specifically, T cells respond to α-syn variants associated with PD and then migrate into the brain where they affect the phenotype of microglia [31]. Viral overexpression of α-syn induces microglia to express major histocompatibility complex II (MHC II) and to present antigens to $CD4^+$ T cells [8,32]. The interactions between T cells, microglia, and pathogenic α-syn are still not well understood. It has been difficult to interrogate the roles of the different populations of immune cells in a model of α-synucleinopathy, as it has been done for other diseases (e.g., Multiple Sclerosis [33]). We addressed this gap in knowledge by triggering α-syn pathology in immunocompromised (NOD scid gamma: NSG, lacking T, B and Natural Killer cells) mice and reconstituting select populations of immune cells. Specifically, we injected protofibrillar human α-syn (PFFs) into the striatum of control mice, NSG mice and NSG mice where T or B cell populations had been reconstituted. We assessed pathological accumulation of phosphorylated α-syn in multiple brain regions and found that NSG mice displayed elevated pathology, while the reconstitution of T cells, but not B cells, in NSG mice was associated with partial reduction of α-syn neuropathology.

MATERIALS AND METHODS

Study design

The goal of our study was to define how a compromised immune system influences the accumulation of pathological α-syn in the brain *in vivo*. To this end, we assessed phosphorylated α-syn pathology following intrastriatal injections of human α-syn PFFs in immunocompromised and control mice. First, we established whether the PFFs injection in the striatum of immunocompromised mice resulted in altered α-syn pathology when compared to wildtype mice. Second, we determined the effects of reconstituting T cells in immunocompromised mice that had received striatal PFFs.

Animals

We utilized 10 to 12-week-old female C57BL/6J, NOD/ShiLtJ (non-obese diabetic) and NSG mouse [immunocompromised, lacking T, B and Natural Killer (NK) cells] mice for injections, and additionally isolated T and B cells from female C57BL/6J mice (bred in our internal vivarium colony). Mice were housed at a maximum of five per cage under a 12-h light/12-h dark cycle with access to food and water *ad libitum*. The housing of the animals and all procedures were carried out in accordance with the *Guide for the Care and Use of Laboratory Animals* (United States National Institutes of Health) and were approved by the Van Andel Research Institute's Institutional Animal Care and Use Committee (AUP 16-12-033). NSG mice carry two mutations on the NOD/ShiLtJ genetic background (severe combined immune deficiency (*scid*) and a complete null allele of the IL2 receptor common gamma chain –*IL2rg*^{null}) [34]. The *scid* mutation renders the mice B and T cell deficient whereas the *IL2rg*^{null} mutation leads to a deficiency in functional NK cells. As the genetic background of the NSG mice is the NOD/ShiLtJ strain [35], NOD mice were used in the first experiment for comparison. NOD mice have defective macrophage maturation and function, low levels of NK cell activity, defects in NKT cells, deficiencies in the regulatory $CD4^{+}CD25^{+}$ T cell population and absence of C5a and hemolytic complement [36].

Purification of recombinant α-synuclein and assembly of pre-formed fibrils

Recombinant human α-syn was purified similarly to this previously published protocol [37,38]. Briefly, the protein was expressed in BL21 *E.coli* transformed with a plasmid expressing human α-syn. Once expressed, cells were collected and stored at -80ºC. For purification, cells were lysed by sonication and boiling, and centrifuged to remove cell debris. The α-syn-containing supernatant was dialyzed overnight in 10 mM Tris, pH 7.5, 50 mM NaCl, and 1 mM EDTA, using SnakeSkin Dialysis Tubing MWCO 7,000 (Thermo Scientific). Chromatographic separation was performed using a Superdex 200 Column (GE Healthcare Life Sciences) and a Hi-trap Q HP anion exchange column (GE Healthcare Life Sciences). Fractions containing α-syn were identified by SDS-PAGE and Coomassie staining, and then dialyzed overnight into PBS buffer (Life Sciences). A NanoDrop 2000 (Thermo Fisher) was used to determine the protein concentration by OD_{280} reading and protein was concentrated to 5 mg/mL using a Vivaspin protein concentrator spin column with a MWCO of 5kDa (GE Healthcare). Aliquots of 500 µL were stored at -80ºC until use. For amyloid fibril assembly, purified recombinant α-syn was thawed and subjected to continuous shaking at 1,000 r.p.m at 37˚C in a Thermomixer (Eppendorf) for 7 days. The monitoring of fibril assemblies was performed by Thioflavin T (Sigma) fluorescence reading (data not shown). Fibrils were aliquoted and frozen at -80˚C until use.

Stereotactic injections

Prior to injection, human α-syn PFFs were thawed and sonicated at RT in a water-bath cup-horn sonicator (Misonix XL2020, 50% power, 120 pulses 1 s ON, 1 s OFF for two minutes). Following sonication, we then

prepared transmission electron microscope grids and stained the PFFs negatively with 1% uranyl acetate to control the morphology of the fibrils prior to injection. Grids were imaged using a Tecnai G2 Spirit TWIN transmission electron microscope at 120kV (FEI Company, Figure 1a). Mice were anesthetized with an isoflurane/oxygen mixture and injected unilaterally with either 2 µL of PFFs (5 µg/µL) or 2 µL of saline as a control in the dorsal striatum (coordinates from bregma: AP: + 0.2 mm; ML: -2.0 mm; DV: - 2.6 mm from dura) at a rate of 0.2 µL/min using a glass capillary attached to a 10 µL Hamilton syringe. After injection, the capillary was left in place for 3 minutes before being slowly removed.

Adoptive transfer

Splenocytes obtained from wildtype mice were transferred i.p. ($1x10^7$ cells/mouse) into NSG mice 4 weeks post PFFs injection. The optimal number of T and B cells for adoptive transfer ranges from $1x10^6$ - $1x10^7$ cells/mouse [39-44]. Purification of T and B cells from total splenocytes was carried out by negative selection using Dynabeads untouched mouse T cells and Dynabeads untouched CD43 B cells isolation kits according to the manufacturer's instruction (Invitrogen). Successful transfer of splenocytes was confirmed by flow cytometric analysis of blood and spleen at the conclusion of the study.

Euthanasia

Mice were deeply anesthetized with sodium pentobarbital at 12 weeks post PFFs-injection. First, the spleen was rapidly collected and kept on ice and blood was collected in 0.5mM EDTA/100 µL of blood. and kept at RT until flow cytometric analysis. Mice were then transcardially perfused with 0.9% saline followed by 4% paraformaldehyde in phosphate buffer. Brains were collected and post-fixed for 24 hours in 4% PFA, and then stored at 4˚C in 30% sucrose in phosphate buffer until sectioning.

Flow cytometric analysis

Immunophenotyping of isolated blood and splenocytes was performed. Blood was collected by cardiac puncture using a 26G needle. A minimum of 300 µL was collected into microfuge tubes containing 0.5mM EDTA/100 µL of blood. Blood was lysed using 1x RBC lysis buffer (eBioscience), spun 300 x g for 10 mins, and the pellet was resuspended in flow buffer: PBS (minus Ca^{2+}/ Mg^{2+}, 2% fetal bovine serum) to bring cell number to ~$5x10^6$ cells/mL. Staining of blood cells were performed on 50 µL of blood incubated with antibodies for 30 mins, RT; SuperBright 702 anti-mouse CD45.1 (clone A20 , 0.5 µg, Invitrogen) or PE-Dazzle595 anti-mouse CD45.1 (clone A20, 0.5 µg, BioLegend), monoclonal anti-mouse CD45.2 APC (clone 104, 0.125 µg, BioLegend), FITC anti mouse CD3ε (1 µg, Clone 145-2C11, BioLegend) and PE anti-mouse CD19 (clone 6D5, 0.5 µg, BioLegend). For splenocyte isolation and staining, spleens were isolated from mouse and kept on ice. In cold 1x RBC lysis buffer (eBioscience), spleens were macerated with the base of a 3 mL syringe plunger on a 70 µm cell strainer in a 10 cm petri dish on ice. 30 mL of PBS was added to stop the reaction. Cells were spun at 350 x g for 5 mins

at 4°C. Pellet was resuspended in 1 mL of PBS for ~$5x10^6$ cells/mL. Staining of splenocyte cells was performed on 100 µL cells as described for blood. Following antibody incubation, blood and spleen cells were washed in flow buffer and spun at 300 x g for 10 mins. Pellets were resuspended in 300 µL of flow buffer with 1 µg/mL DAPI. Samples were acquired on a CytoFLEX S (BeckmanCoulter). Data analysis was performed using FlowJo v10.5.3. First, DAPI-negative live cells were gated, followed by single cells as identified on a plot of SSC-A vs SSC-H. C57Bl6J mice are positive for CD45.2 while NSG mice express CD45.1. We gated on $CD45.2^+$ cells, then subsetted them into $CD3^+$ and $CD19^+$ to identify T and B cells in the blood or spleen originating from the wildtype lineage.

Histology

Brains were sectioned into 40 µm-thick free-floating coronal sections using a freezing microtome. Brain sections were stored in cryoprotectant and quenched with sodium peroxide. During the staining protocols, sections were incubated at room temperature overnight with primary antibodies directed against phosphorylated α-syn (rabbit anti-pS129, Abcam) at 1:10000 dilution, microglia (rabbit anti-Iba-1, WAKO) at 1:500 dilution, and an antibody to tyrosine hydroxylase (TH, rabbit, 1:1600, EMD Millipore). Sections containing the substantia nigra were stained for TH and mounted onto gelatin coated slides for stereological assessment of cell counts, and counter-stained with Cresyl violet for assessment of $Nissl^+$ cells. To detect $CD3^+$ in the striatum, substantia nigra and frontal cortex of mice, we used a heat induced antigen retrieval protocol using a Universal HIER antigen retrieval reagent (Abcam). Sections were incubated with rat anti-CD3 (Abcam) at 1:100 dilution. Sections were incubated with rabbit or rat biotinylated secondary antibodies (Vector Laboratories) and conjugated with an ABC-HRP biotin/avidin complex kit (Vector Laboratories). Staining was developed with 3,3′-diaminobenzidine then sections were mounted for imaging and analysis. Representative images of phosphorylated α-syn pathology and microglia were acquired at 20x magnification using a Nikon Eclipse Ni-U microscope.

Immunofluorescence

To detect $CD4^+$ cells we used heat induced antigen retrieval (as detailed above). Sections were incubated with rabbit anti-CD4 (Abcam) at 1:100 dilution. Next, sections were treated with donkey anti-rabbit Alexa 594 (1:500 dilution, Invitrogen) with DAPI (1:10000 dilution) added to the secondary solution. Sections were mounted and coverslipped using Vectashield mounting medium (Vector Laboratories) Representative images of $CD4^+$ were acquired at 20x magnification using a Nikon Eclipse Ni-U microscope.

Densitometry of phosphorylated α-syn pathology

We investigated phosphorylated α-syn pathology in the ipsilateral striatum, substantia nigra and frontal cortex of mice injected with human α-syn PFFs by densitometry. Briefly, we acquired photomicrographs from slides at 20x magnification on three consecutive sections, three images per section, distanced by a 240 µm interval. Striatal

images, were captured at the level of bregma +0.26 mm, the images from the substantia nigra were captured from bregma -3.08 mm and the frontal cortex images from bregma +3.20 mm [45]. The images were then analyzed in ImageJ64 (Rasband WS (1997) ImageJ (modified in 2016) NIH, Bethesda, Maryland, USA). Images were converted to 8-bit grayscale, images thresholded and particles analyzed to obtain the area and the mean grey value (A.U.) of the phosphorylated α-syn-positive area. We determined the average grey value in this area in each brain region and animal. We then normalized to the PFFs injected wildtype mice (value as 1) and plotted the groups as a fold change from the PFFs injected wildtype group.

Assessment of microglial morphology

Microglia morphology was assessed as previously described [46]. Color (RGB) images of Iba-1-stained striatal, substantia nigra and frontal cortex tissues were acquired at 60x magnification (oil immersion 1.40 N.A.) using a Nikon Eclipse Ni-U microscope. A total of nine images/animal were analyzed; three images from three sequential brain sections through the striatum (as described above). To assess the morphology of microglia in the samples, RGB color images were processed by a custom MATLAB (Mathworks) script. Cell bodies and other large regions were segmented first. Dynamic thresholds were determined for both the blue intensity and saturation channels of the image. Upper and lower bounds of the thresholds were set to match the full width at half maximum of curves fit to the histograms of each channel. If the signal met the required criteria for either the blue channel or the saturation channel thresholds, it was selected for further analysis. Segmented regions were filtered to remove small (under 2,000-pixel) areas and to remove objects that touched the borders of the image. The segmented areas were eroded to more accurately conform to cell bodies. The ratio of area:perimeter (referred to as hydraulic radius) was calculated and used as a measure for microglial activation; activated microglia are amoeboid in shape and therefore exhibit a larger index score.

Stereological counting

We used a computer-assisted cell quantification program (StereoInvestigator, MBF Bioscience) coupled to a Nikon Eclipse Ni-U microscope (Nikon). In each mouse (3–4 animals per group), we analyzed 5–7 sections containing substantia nigra. They were spaced by 240 µm (section interval = 6). Contours of the region were drawn at 10x magnification (air immersion, N.A. 0.45). Quantifications were performed at 60x (oil immersion, N.A. 1.40) using a counting frame of 100 µm × 100 µm, grid size set to 200 × 200 µm, with a guard zone of 2 µm, and dissector height set at 12 µm.

Statistical analysis

All values are expressed as mean ± SEM. Differences in means between the groups were analyzed using a Pairwise Wilcoxon Rank Sum Tests or one-way ANOVA test by using R software (v 3.6.2) and GraphPad Prism software, respectively. A p value < 0.05 was considered statistically significant.

RESULTS

Increased phosphorylated α-syn inclusions in NSG PFFs injected mice

To determine the influence of a compromised immune system in the accumulation of phosphorylated α-syn following injection of fibrillar α-syn into the striatum, we compared NSG mice to NOD/ShiLtJ and to wildtype mice. NOD/ShiLtJ mice were used for the primary comparison as they are the background strain to NSG mice. In addition, NOD/ShiLtJ mice were also as they are a model of immunodeficiency [36]. The timeline of the experiment is represented in Figure 1a. The sizes of the generated PFFs were verified by transmission electron microscopy (Figure 1b), and they were consistent with the PFFs we have used previously in our laboratory [38].

The accumulation of phosphorylated α-syn inclusions in wildtype, NOD and NSG mice four weeks after a single intrastriatal injection with recombinant human α-syn PFFs are presented in Figure 1. Pathology in three brain regions, the ipsilateral striatum, substantia nigra and frontal association cortex (referred to as frontal cortex from hereon, see Figure 1c for representative images of pathology), was selected for quantification. In all graphs, the levels of phosphorylated α-syn were normalized to the average level of pathology in the wildtype mice injected with α-syn PFFs and plotted as a fold change.

In the striatum and substantia nigra, NSG mice inoculated with α-syn PFFs displayed significantly more pathology compared to α-syn PFFs-injected wildtype mice, but not when compared to NOD mice injected with α-syn PFFs ($p < 0.05$, Figure 1c and 1d). In the frontal cortex, the levels of phosphorylated α-syn pathology were increased in PFF-injected NSG mice compared to wildtype PFFs-injected mice but this did not reach significance ($p = 0.0539$, Figure 1d).

As mentioned above, NOD/ShiLtJ mice have multiple immune cell dysfunctions including T cell deficits, defects in innate immunity like reduced dendritic cell function, lack of mature NK cells and defective macrophage activity as well as neuroinflammatory changes [35,36,47]. NOD/ShiLtJ mice also spontaneously develop type I diabetes (43%-80% by 30 weeks of age) [36,48-50]. As the phosphorylated α-syn load in the NOD/ ShiLtJ mice was not significantly different to NSG PFFs-injected mice, this supports the hypothesis that immune defects lead to increased phosphorylated α-syn pathology. In addition, to overcome the potential problem of NOD/ShiLtJ mice developing type I diabetes, we injected NSG mice with PFFs for the remainder of the study. Using NSG PFFs-injected mice allowed us to specifically address the aim of whether T or B cells influence the accumulation of phosphorylated α-syn inclusions. We used wildtype mice as the donors of the T and B cells and for comparison for the remainder of the study.

Decreased phosphorylated α-syn in NSG mice reconstituted with T cells

Above we established that there is increased α-syn related pathology following striatal PFFs injections in NSG mice compared to wildtype mice. We then investigated whether reconstituting the T cell population in PFFs-injected NSG mice would alter the phosphorylated α-syn levels in the striatum, the substantia nigra or frontal cortex. Throughout the manuscript, we refer to NSG mice injected with human α-syn PFFs and reconstituted with T cells as NSG PFF T and NSG mice injected with human α-syn PFFs and reconstituted with B cells as NSG PFF B. The reconstitution of T cells was conducted in two separate experiments and the results were pooled after we determined that there was no difference in the neuropathological outcomes between the two experiments (data not shown). Mice were injected with PFFs in the striatum; four weeks later, the adoptive transfer of immune cells was performed. Pathology was assessed 12 weeks post PFFs injection. Flow cytometry plots from the blood and splenocytes isolated from the reconstituted NSG mice were positive for $CD3^+$ $CD45.2^+$ T cells. C57Bl/6J mice express the CD45.2 allele while NSG mice express the CD45.1 allele (representative plots in Figure 2a), therefore CD45.2 positive cells demonstrated the successful uptake of donated T cells. We observed $CD3^+$ cells in the striatum, substantia nigra and frontal cortex in PFFs injected mice that were reconstituted with T cells (Figure 2c). As CD3 is also expressed on NK cells, we confirmed the presence of $CD4^+$ T cells in the striatum, substantia nigra and frontal cortex by immunofluorescence (Figure 2c).

It was clear that the PFFs-injected NSG mice exhibited increased phosphorylated α-syn pathology compared to PFFs-injected wildtype mice in the substantia nigra and frontal cortex and not in the striatum (Figure 3b, c, $p < 0.05$). The experimental timeline is represented in Figure 3a. Interestingly, reconstituting T cells in NSG PFFs injected mice significantly decreased levels of phosphorylated α-syn in the substantia nigra when comparing NSG PFFs to NSG PFF T mice (Figure 3b, c, $p < 0.05$). The levels of phosphorylated α-syn in the striatum and frontal cortex following T cell reconstitution decreased, but did not reach significance (Figure 3c, $p > 0.05$).

As a control experiment for the reconstitution of T cells, we reconstituted a different group of NSG mice with B cells (timeline of experiment represented in Figure 4a). B cells on their own are not expected to affect pathology as they need T cells to work in concert for an antibody response [36,48-50]. Therefore this was a control experiment to determine the effect of the reconstitution per se. The transfer of B cells was confirmed by flow cytometry (Figure 4b). Consistent with the above results, there was an increase in phosphorylated α-syn in the striatum, substantia nigra and frontal cortex in PFFs-injected NSG mice compared to PFFs-injected wildtype mice, but this did not reach significance ($p > 0.05$, Figure 4c, d). The increase in phosphorylated α-syn pathology in the striatum and substantia nigra in the wildtype PFFs-injected mice compared to NSG PFF B did reach significance (Figure 4c, d, $p < 0.05$). In the striatum, substantia nigra and frontal cortex, the levels of phosphorylated α-syn pathology in the PFFs-injected NSG mice following the transfer of B cells did not significantly change (Figure 4c, d).

Microgliosis in mice reconstituted with T cells

To understand whether microglia were involved in the reduction of phosphorylated α-syn pathology in NSG mice reconstituted with T cells, we analyzed the morphology of microglia. We immunostained for Iba-1 to compare microglial morphology between all groups (Figure 5). We compared the morphology of Iba-1 immunoreactive microglia from the same anatomical level in the striatum in mice from each experimental group. Specifically, we used a MATLAB script to define the ratio between the perimeter and surface area of Iba-1-immunoreactive microglia within the striatum, allowing us to calculate the hydraulic radius of each cell as an index of the activation state (Figure 5a). The area:perimeter index (hydraulic radius) measures microglial activation as activated microglia are amoeboid in shape. Thus, these activated cells have a large area and small perimeter, increasing the index score. An example of activated microglia with an amoeboid shape is in Figure 5c. The hydraulic radius was significantly increased in microglia from within the striatum of NSG PFFs injected mice that received T cells relative to wildtype Saline, wildtype PFFs, NSG Saline, NSG PFFs, NSG PFF T and NSG PFF B cell injected mice (Figure b, $p < 0.05$) indicating that microglia in the NSG PFF T group are activated. The hydraulic radius of microglia analyzed from the substantia nigra was not significantly different between the groups (Figure 5b, $p > 0.05$). In the frontal cortex, the hydraulic radius of microglia in the NSG PFF B mice was significantly reduced compared to the NSG PFF T mice (Figure 5b, $p < 0.05$).

To determine whether adoptive transfer of T cells altered the number of dopaminergic cells in the substantia nigra, we performed stereological cell counts from wildtype saline, wildtype PFFs-injected and NSG saline and NSG PFFs-injected mice and from NSG mice reconstituted with T and B cells. We determined that PFFs injection resulted in significant cell loss in TH-positive neurons (Figure 5d, significant main effect of hemisphere, $p <0.05$) and that reconstitution of T or B cells was not significantly different from the cell loss observed in the NSG PFFs-injected mice (Figure 5d, $p >0.05$).

DISCUSSION

We explored the role of T cells in the accumulation of α-syn following intracerebral inoculation with α-syn fibrils in immunocompromised mice (NSG) that lack B, T and natural killer cells [34]. Compared to wildtype mice injected with α-syn fibrils into the striatum, NSG mice injected with PFFs developed greater accumulation of phosphorylated α-syn in the striatum, substantia nigra and frontal cortex. To identify whether the absence of T lymphocytes was driving this elevation in phosphorylated α-syn inclusions, we reconstituted NSG mice with T cells via adoptive transfer four weeks after intrastriatal injections of α-syn PFFs. To control for the injection of immune cells via adoptive transfer, we injected a separate group of mice with B cells isolated from wildtype mice. Notably, the transfer of T cells resulted in a significant decrease in phosphorylated α-syn immunostaining in the substantia nigra but not in the striatum and frontal cortex, where only a trend was observed. Our data directly

link T cells and the development of nigral α-syn neuropathology *in vivo*. This complements several reports associating altered T cell function with PD and MSA [22-27,51] and studies demonstrating activation of immune cells by pathogenic α-syn [28,30,52]. One such study measuring nigral neurodegeneration as the readout of the model supports the hypothesis that immune cells can modulate neuroinflammation and neurodegeneration in PD mouse models [53]. Viral overexpression of human α-syn in the substantia nigra of immune competent mouse results in microglial activation, MHC II activation, T cell and monocyte entry into the brain and consequently, loss of substantia nigra neurons [32,54,55].

Our findings support these prior studies by showing that intrastriatal injection of human α-syn PFFs leads to elevated phosphorylated α-syn pathology in immunodeficient compared to wildtype mice. We found that this exacerbation of pathology was partially mitigated by adoptive transfer of T cells into the immunodeficient NSG mice that received intrastriatal injections of human α-syn PFFs. Further, following adoptive transfer we observed $CD3^+$ and $CD4^+$ T cells in the striatum, substantia nigra and frontal cortex which supports previous work showing infiltration of T cells in PD brains and in a neurotoxin model of nigral neurodegeneration [21,56]. Our findings of $CD3^+$ and $CD4^+$ T cells in the brain align with a growing body of evidence that T cells can travel from the periphery to the central nervous system [57,58].

We also investigated whether the decrease in pathology observed following adoptive transfer of T cells could be due to cytotoxic T cells killing neurons that exhibit phosphorylated α-syn, leading to an apparent reduction of α-syn staining as a consequence. This idea would be consistent with an earlier study showing that mice lacking $CD4^+$ T cells are relatively resistant to MPTP-induced degeneration of substantia nigra dopamine neurons [56]. However, we did not find this to be the explanation for the reduction in α-syn pathology. Stereological counts of dopaminergic neurons of the substantia nigra revealed similar reductions in nigral TH-immunoreactive neurons following intrastriatal injection of α-syn PFFs in mice lacking T cells as those having their T cell population reconstituted (Figure 5d). The contrast to other findings could be due to the timeline and the species of α-syn that is inducing the pathology in our model.

An alternative mechanism for the significant decrease in phosphorylated α-syn following T cell reconstitution is that the infiltration of T cells leads to the activation of microglia and that these resident macrophages remove phosphorylated α-syn. Earlier studies have also shown that T cells invading the brain can activate microglia [57-60]. Indeed, we also found microglia morphology was significantly altered in the striatum of mice that received adoptive transfer of T cells following intrastriatal injection of α-syn PFFs. The microgliosis that we observed was restricted to the striatum in line with previous work in immunocompetent rats [61]. Microglia are heterogenous and have distinct region-dependent transcriptional identities, where the local environment influences the molecular and morphological profiles of microglia [62-64]. It is therefore possible that the response to human α-syn is region-

specific, with striatal microglia becoming more highly activated than microglia in the substantia nigra and frontal cortex in this paradigm.

Our study did not address the influence of NK cells in the accumulation of phosphorylated α-syn inclusions. NK cell function is altered in peripheral lymphocytes obtained from PD patients as the levels of inhibitory receptors on NK cells are significantly lowered in PD patients, rendering the NK cells more susceptible to activation [65]. NK cells are one of the first lines of defense of the innate immune system [66]. They respond rapidly to a variety of insults with cytolytic activity and cytokine secretion [67]. They are implicated in diseases of autoimmunity and within the CNS, in an autoimmune context, NK cells can interact with microglia [67]. Recently, it was reported that systemic depletion of NK cells in a preclinical model of PD exacerbated the α-syn pathology observed in this model [68]. The preclinical model utilized α-syn transgenic mice that over-express human α-syn with the A53T mutation in addition to an injection of human α-syn PFFs into the dorsal striatum. The depletion of NK cells in this model of α-syn-induced pathology suggests that NK cells can contribute to the clearance of α-syn aggregates or prevent their formation [68]. The mice we used in our study also have deficiencies in NK cells. Mice that have a mutation in the interleukin-2 receptor common gamma chain, such as the NSG mice used in this study, have interrupted cytokine signaling networks for multiple cytokines, in particular Interleukin-15, which contributes to a complete lack of NK cells [69]. Thus, the NOD/ShiLtJ mice have dysfunctional NK cells and NSG mice lack NK cells all together [34,36,69]. Notably, we found that phosphorylated α-syn was increased in multiple brain regions in both NOD/ShitLtJ mice and NSG mice when compared to wildtype mice in Figure 1. In light of the recent findings mentioned above [68], a driver of this difference between wildtype and the mice on the NOD background could be the dysfunctional or absent NK cells. With the dysregulation or loss of NK cells in our model, it can be postulated that both arms of immunity are needed to modulate levels of phosphorylated α-syn accumulation. To clarify the specific role of NK cells in α-synucleinopathy, future studies are needed where NK cells are reconstituted in the immunocompromised mice.

Our results highlight the role for the adaptive immune system, and specifically T cells, in the accumulation of α-syn. We did not, however, investigate the dynamics of the microglial response and accumulation of phosphorylated α-syn. To further delineate the role for T and B cells in the accumulation of α-syn in a PD relevant paradigm, experiments transferring T and B cells from wild type PFFs-injected mice that have been previously exposed to human α-syn PPFs would be informative. This would also allow us to define the role of B cells, as B cells require T cells for their maturation and for the production of antibodies [70]. In the current study, we injected naïve B-cells from wild-type mice that have never been presented to human α-syn PFFs, therefore the B cells lack the specific receptors for this antigen.

CONCLUSION

Compared to wildtype mice injected with PFFs into the striatum, NSG immunocompromised mice injected with PFFs exhibited increased phosphorylated α-syn levels in the substantia nigra and not in the striatum and frontal cortex. The accumulation of phosphorylated α-syn in the substantia nigra was reduced when we used adoptive transfer to reconstitute the T cell population in the immunocompromised mice. We observed signs of elevated microglia activation in the striatum in mice that received the T cell adoptive transfer. Taken together, our study provides direct *in vivo* evidence that T cells modulate accumulation of phosphorylated α-syn and supports an important role for the immune system in the PD pathogenesis.

List of abbreviations

MHC II: major histocompatibility complex II

NOD/ShiLtJ (NOD): Non-obese diabetic

NSG: NOD Scid gamma

PD: Parkinson's disease

PFFs: preformed fibrils

α-syn: α-synuclein

Declarations

Availability of data and materials

All data generated during this study are included in this published article.

Competing interests

PB has received commercial support as a consultant from Axial Biotherapeutics, CuraSen, Fujifilm-Cellular Dynamics International, IOS Press Partners, LifeSci Capital LLC, Lundbeck A/S and Living Cell Technologies LTD. He has received commercial support for grants/research from Lundbeck A/S and Roche. He has ownership interests in Acousort AB and Axial Biotherapeutics and is on the steering committee of the NILO-PD trial. The authors declare no additional competing financial interests.

Funding

This work was supported by the Farmer Family Foundation and S.G. was supported by the Peter C. and Emajean Cook Foundation.

Authors' contributions

SG designed the study, performed the surgeries, adoptive transfer, prepared samples for flow cytometry, the immunohistochemistry, acquisition of brightfield images, and MATLAB and image analysis, interpreted the histological results, and wrote the manuscript. TT contributed to the design of the study, assisted in the isolation

of cells for adoptive transfer and edited the manuscript. NLR assisted in the NOD and NSG PFFs surgeries and edited the manuscript. RS acquired and analyzed the flow cytometry data. WP performed the Iba-1 and CD4 immunostaining. KB generated the PFFs. ES and LM assisted with perfusions and performed immunohistochemistry. ARB assisted with the adoptive transfer. MLEG, JAS, and LB edited the manuscript and contributed to interpretation of the results. JM provided the PFFs and edited the manuscript. PB contributed to the design of the study and interpretation of the results and edited the manuscript. All authors gave input to the manuscript. All authors read and approved the final manuscript.

Acknowledgements

We thank Dr. Corinne Esquibel from the Optical Imaging core for developing the MATLAB algorithm for microglia morphology analysis, Emily Wolfrum from the Bioinformatics and Biostatistics for assistance with the statistical analysis and the staff of the Vivarium of Van Andel Research Institute for animal care. We acknowledge the Van Andel Research Institute and the many individuals and corporations that supported financially the neurodegenerative research at Van Andel Research Institute. S.G. was supported by the Peter C. and Emajean Cook Foundation and the Farmer Family Foundation.

Research reported in this publication was supported by the National Institute On Deafness And Other Communication Disorders of the National Institutes of Health under Award Numbers R01DC016519 (P.B.) and the National Institute of Neurological Disorders and Stroke of the National Institutes of Health under Award Numbers R21NS106078-01A1 (P.B.). The content is solely the responsibility of the authors and does not necessarily represent the official views of the National Institutes of Health.

We would like to acknowledge iPark and the Farmer Family Foundation for funding a portion of this work.

Figure legends

Figure 1. Increased phosphorylated α-syn pathology in immunocompromised mice injected with human α-syn pre-formed fibrils. a. Timeline of the experiment. b. PFFs were sonicated and validated by transmission electron microscopy. c. α-Syn pathology in the injected striatum was detected in the ipsilateral striatum, substantia nigra and ipsilateral frontal cortex at 4 weeks post injection, by an antibody against phosphorylated α-syn at serine 129. d. Densitometry performed on 4-10 animals per group in the striatum, substantia nigra and frontal cortex (wildtype Saline, n = 4; wildtype PFFs, n = 4; NOD PFFs, n = 6; NSG PFFs n = 10). Statistical analyses were performed by Pairwise Wilcoxon Rank Sum Tests analysis* $p < 0.05$, ** $p < 0.01$, Scale bar: 100 μm.

Figure 2. T cells in the blood, spleen and brain following adoptive transfer. a. Flow cytometric analysis. Wildtype mice contained populations of T and B cells that are CD45.2 positive. NSG mice did not contain T and B cell populations. Following adoptive transfer of T cells to NSG mice, $CD45.2^+$ $CD3^+$ T cells were detected.

Representative plots are shown for each treatment condition. b. Representative images from the mouse striatum, substantia nigra and frontal cortex staining positive for $CD3^+$T cells in mice that received adoptive transfer of T cells. c. Immunofluorescent staining for $CD4^+$ T cells in the striatum, substantia nigra and frontal cortex. Scale bar: 100 μm.

Figure 3. Reduced phosphorylated α-syn pathology in immunocompromised mice that received adoptive transfer of T cells. a. Timeline of experiment. b. Phosphorylated α-syn was detected in the ipsilateral striatum, substantia nigra and frontal cortex. The reconstitution of T cells was conducted in two separate experiments and the results pooled after results of the reduction in phosphorylated α-syn were shown to be consistent between the two experiments. c. Densitometry of 5-9 mice per group to determine the fold change in phosphorylated α-syn levels in the ipsilateral striatum, substantia nigra and frontal cortex. Wildtype Saline, n=5; NSG Saline n=5, wildtype PFF, n=6; NSG PFF, n=6; NSG PFF T n=7). d. Statistical analyses were performed by Pairwise Wilcoxon Rank Sum Tests analysis * $p<0.05$, ** $p<0.01$. Scale bar: 100 μm.

Figure 4. Adoptive transfer of B cells alone did not alter phosphorylated α-syn pathology in immunocompromised mice. a. Timeline of experiment. b. Flow cytometric analysis of mouse spleen and blood following adoptive transfer demonstrated that wildtype mice contain populations of T and B cells that are CD3 and CD19 positive. NSG mice do not have T and B cell populations. Following adoptive transfer of B cells, NSG mice contained $CD45.2^+$ $CD19^+$ B cells. Representative plots are shown for each treatment condition. c. Phosphorylated α-syn was detected in the ipsilateral striatum, substantia nigra and frontal cortex. d. Densitometry of 3-9 mice per group to determine the fold change in phosphorylated α-syn levels in the ipsilateral substantia nigra. Wildtype Saline, n = 5; NSG Saline n = 3, wildtype PFFs, n = 3; NSG PFFs, n = 3; NSG PFF B n = 9). The error bars represent S.E.M. Statistical analyses were performed by Pairwise Wilcoxon Rank Sum Tests analysis ** $p < 0.01$. Scale bar: 100 μm.

Figure 5. Microgliosis and dopaminergic cells death in the brain of α-syn PFFs injected mice. a. Representative images of Iba-1 immunoreactive microglia were present in the ipsilateral striatum, substantia nigra and frontal cortex of saline and PFFs injected mice. b**.** Quantification of microglia morphology (area/perimeter). Wildtype Saline, n = 5; NSG Saline n = 4, wildtype PFFs, n = 10; NSG PFFs, n = 3; NSG PFF T n = 4; NSG PFF B n = 4). c. Example of the microglia Matlab morphology algorithm. Individual microglia were identified in the original image by red dots. The user identifies which cells are used for analysis. d. Stereological counts of saline and PFFs injected wildtype and NSG mice. There was no main effect of genotype ($p > 0.05$), but a significant main effect of hemisphere ($p < 0.05$) in the total number of TH-expressing cells in the substantia nigra between contralateral substantia nigra (black bars) and ipsilateral substantia nigra

(grey bars). The error bars represent S.E.M. Statistical analyses were performed by one and two-ANOVA analysis * $p < 0.05$, ** $p < 0.01$, *** $p < 0.001$. Scale bar: 100 μm.

References

1. Selkoe, D. *et al.* Defining the native state of α-synuclein. *Neurodegenerative dis* **13,** 114–117 (2014).
2. Hirsch, E. C. & Hunot, S. Neuroinflammation in Parkinson's disease: a target for neuroprotection? *Lancet Neurol* **8,** 382–397 (2009).
3. Wakabayashi, K., Yoshimoto, M., Tsuji, S. & Takahashi, H. α-Synuclein immunoreactivity in glial cytoplasmic inclusions in multiple system atrophy. *Neurosci. Lett.* **249,** 180–182 (1998).
4. Rydbirk, R. *et al.* Cytokine profiling in the prefrontal cortex of Parkinson's Disease and Multiple System Atrophy patients. *Neurobiol Dis* **106,** 269–278 (2017).
5. Steiner, J. A., Quansah, E. & Brundin, P. The concept of alpha-synuclein as a prion-like protein: ten years after. *Cell Tissue Res* **373,** 161–173 (2018).
6. Zhang, W. *et al.* Aggregated alpha-synuclein activates microglia: a process leading to disease progression in Parkinson's disease. *FASEB J* **19,** 533–542 (2005).
7. Lee, H.-J., Bae, E.-J. & Lee, S.-J. Extracellular α-synuclein—a novel and crucial factor in Lewy body diseases. *Nat Rev Neurol* **10,** 92–98 (2014).
8. Kim, C. *et al.* Neuron-released oligomeric α-synuclein is an endogenous agonist of TLR2 for paracrine activation of microglia. *Nat Comms* **4,** 1562–1562 (2013).
9. Gerhard, A. *et al.* In vivo imaging of microglial activation with [11C](R)-PK11195 PET in idiopathic Parkinson's disease. *Neurobiol Dis* **21,** 404–412 (2006).
10. Mogi, M. *et al.* Interleukin (IL)-1 beta, IL-2, IL-4, IL-6 and transforming growth factor-alpha levels are elevated in ventricular cerebrospinal fluid in juvenile parkinsonism and Parkinson's disease. *Neurosci. Lett.* **211,** 13–16 (1996).
11. Mogi, M. *et al.* Tumor necrosis factor-alpha (TNF-alpha) increases both in the brain and in the cerebrospinal fluid from parkinsonian patients. *Neurosci. Lett.* **165,** 208–210 (1994).
12. Brodacki, B. *et al.* Serum interleukin (IL-2, IL-10, IL-6, IL-4), TNFα, and INFγ concentrations are elevated in patients with atypical and idiopathic parkinsonism. *Neurosci. Lett.* **441,** 158–162 (2008).
13. Compta, Y. *et al.* Cerebrospinal fluid cytokines in multiple system atrophy: A cross-sectional Catalan MSA registry study. *Parkinsonism Relat. Disord.* **65,** 3–12 (2019).
14. Yamasaki, R. *et al.* Early strong intrathecal inflammation in cerebellar type multiple system atrophy by cerebrospinal fluid cytokine/chemokine profiles: a case control study. *J Neuroinflam* **14,** 89–10 (2017).
15. Li, F., Ayaki, T., Maki, T., Sawamoto, N. & Takahashi, R. NLRP3 inflammasome-related proteins are upregulated in the putamen of patients with multiple system atrophy. *J Neuropathol Exp Neurol* **77,** 1055–1065 (2018).
16. Hamza, T. H. *et al.* Common genetic variation in the HLA region is associated with late-onset sporadic Parkinson's disease. *Nat Genetics* **42,** 781–785 (2010).
17. Hirsch, E. C., Vyas, S. & Hunot, S. Neuroinflammation in Parkinson's disease. *Parkinsonism Relat Disord* **18,** S210–S212 (2012).
18. Ransohoff, R. M. How neuroinflammation contributes to neurodegeneration. *Science* **353,** 777–783 (2016).
19. Schwartz, M. & Baruch, K. The resolution of neuroinflammation in neurodegeneration: leukocyte recruitment via the choroid plexus. *EMBO J.* **33,** 7–22 (2014).
20. Brochard, V. *et al.* Infiltration of CD4+ lymphocytes into the brain contributes to neurodegeneration in a mouse model of Parkinson disease. *J. Clin. Invest.* **119,** 182–192 (2009).
21. Hickey, W. F. Basic principles of immunological surveillance of the normal central nervous system. *Glia* **36,** 118–124 (2001).

22. Baba, Y., Kuroiwa, A., Uitti, R. J., Wszolek, Z. K. & Yamada, T. Alterations of T-lymphocyte populations in Parkinson disease. *Parkinsonism Relat Disord* **11,** 493–498 (2005).
23. Hisanaga, K., Asagi, M., Itoyama, Y. & Iwasaki, Y. Increase in Peripheral CD4 Bright+ CD8 Dull+ T Cells in Parkinson Disease. *Arch Neurol* **58,** 1580–1583 (2001).
24. Bas, J. Lymphocyte populations in Parkinson's disease and in rat models of parkinsonism. *J Neuroimmunol* **113,** 146–152 (2001).
25. Saunders J, Estes KA, Kosloski LM, CD4+ regulatory and effector/memory T cell subsets profile motor dysfunction in Parkinson's disease. J Neuroimmune Pharmacol **7**, 927-38 (2012).
26. Stevens, C. H. *et al.* Reduced T helper and B lymphocytes in Parkinson's disease. *J Neuroimmunol* **252,** 95–99 (2012).
27. Chiba, S. *et al.* A correlation study between serum adenosine deaminase activities and peripheral lymphocyte subsets in Parkinson's disease. *J Neurol Sci* **132,** 170–173 (1995).
28. Sulzer, D. *et al.* T cells from patients with Parkinson's disease recognize α-synuclein peptides. *Nature* **546,** 656 (2017).
29. Sommer, A. *et al.* Th17 Lymphocytes Induce Neuronal Cell Death in a Human iPSC-Based Model of Parkinson's Disease. *Stem Cell* **23,** 123–131.e6 (2018).
30. Theodore, S., Cao, S., McLean, P. J. & Standaert, D. G. Targeted overexpression of human alpha-synuclein triggers microglial activation and an adaptive immune response in a mouse model of Parkinson disease. *J. Neuropathol. Exp. Neurol.* **67,** 1149–1158 (2008).
31. Olesen, M. N. *et al.* CD4 T cells react to local increase of α-synuclein in a pathology-associated variant-dependent manner and modify brain microglia in absence of brain pathology. *Heliyon* e00513 (2018).
32. Harms, A. S. *et al.* MHCII Is Required for α-Synuclein-Induced Activation of Microglia, CD4 T Cell Proliferation, and Dopaminergic Neurodegeneration. *J. Neurosci.* **33,** 9592–9600 (2013).
33. Mundt, S., Greter, M., Flügel, A. & Becher, B. The CNS Immune Landscape from the Viewpoint of a T Cell. *Trends Neurosci.* **42,** 667–679 (2019).
34. Shultz, L. D. *et al.* Human Lymphoid and Myeloid Cell Development in NOD/LtSz-scid IL2Rγnull Mice Engrafted with Mobilized Human Hemopoietic Stem Cells. *J Immunol* **174,** 6477–6489 (2005).
35. Shultz, L. D. *et al.* Multiple defects in innate and adaptive immunologic function in NOD/LtSz-scid mice. *J Immunol* **154,** 180–191 (1995).
36. Anderson, M. S. & Bluestone, J. A. THE NOD MOUSE: A Model of Immune Dysregulation. Annu Rev Immunol. **23,** 447–485 (2005).
37. Volpicelli-Daley, L. A., Luk, K. C. & Lee, V. M. Y. Addition of exogenous α-synuclein preformed fibrils to primary neuronal cultures to seed recruitment of endogenous α-synuclein to Lewy body and Lewy neurite–like aggregates. *Nat Protoc* **9,** 2135–2146 (2014).
38. Becker, K. *et al.* Detecting Alpha Synuclein Seeding Activity in Formaldehyde-Fixed MSA Patient Tissue by PMCA. *Mol Neurobiol* **55,** 8728–8737 (2018).
39. Zuccarino-Catania, G. & Shlomchik, M. Adoptive Transfer of Memory B Cells. *Bio Protoc* **5,** (2015).
40. Gautreaux, M. D., Gelder, F. B., Deitch, E. A. & Berg, R. D. Adoptive transfer of T lymphocytes to T-cell-depleted mice inhibits Escherichia coli translocation from the gastrointestinal tract. *Infection and Immunity* **63,** 3827–3834 (1995).
41. Reynolds, A. D. *et al.* Regulatory T Cells Attenuate Th17 Cell-Mediated Nigrostriatal Dopaminergic Neurodegeneration in a Model of Parkinson's Disease. *J Immunol* **184,** 2261–2271 (2010).
42. Ashman, R. B. *Leucocytes: methods and protocols*. Methods Mol Biol. 844:v (2012).
43. Kawahara, T., Ohdan, H., Zhao, G., Yang, Y.-G. & Sykes, M. Peritoneal cavity B cells are precursors of splenic IgM natural antibody-producing cells. *J Immunol* **171,** 5406–5414 (2003).
44. Klenovsek, K. *et al.* Protection from CMV infection in immunodeficient hosts by adoptive transfer of memory B cells. *Blood* **110,** 3472–3479 (2007).
45. Paxinos, G. & Franklin, K. B. J. *The mouse brain in stereotaxic coordinates*. (Academic Press, 2001).
46. George, S. *et al.* Microglia affect α-synuclein cell-to-cell transfer in a mouse model of Parkinson's disease. *Mol Neurodegener*. **14**, 34 (2019).

47. McGuiness, B. *et al.* Exaggerated Increases in Microglia Proliferation, Brain Inflammatory Response and Sickness Behaviour upon Lipopolysaccharide Stimulation in Non-Obese Diabetic Mice. *NIM* **23,** 137–150 (2016).
48. Ize-Ludlow, D. *et al.* Progressive Erosion of -Cell Function Precedes the Onset of Hyperglycemia in the NOD Mouse Model of Type 1 Diabetes. *Diabetes* **60,** 2086–2091 (2011).
49. Mathews, C. E. *et al.* Acute Versus Progressive Onset of Diabetes in NOD Mice: Potential Implications for Therapeutic Interventions in Type 1 Diabetes. *Diabetes* **64,** 3885–3890 (2015).
50. Zhang, Z. J., Davidson, L., Eisenbarth, G. & Weiner, H. L. Suppression of diabetes in nonobese diabetic mice by oral administration of porcine insulin. *Proc. Natl. Acad. Sci. U.S.A.* **88,** 10252–10256 (1991).
51. Williams, G. P. *et al.* T cell infiltration in both human multiple system atrophy and a novel mouse model of the disease. *Acta Neuropathol* 1–20 (2020).
52. Grozdanov, V. *et al.* Increased immune activation by pathologic alpha-synuclein in Parkinson's Disease. *Ann. Neurol.* ana.25557–36 (2019).
53. Williams, G. P. *et al.* Targeting of the class II transactivator attenuates inflammation and neurodegeneration in an alpha-synuclein model of Parkinson's disease. 1–14 (2018).
54. Thome, A. D., Harms, A. S., Volpicelli-Daley, L. A. & Standaert, D. G. microRNA-155 Regulates Alpha-Synuclein-Induced Inflammatory Responses in Models of Parkinson Disease. *J. Neurosci.* **36,** 2383–2390 (2016).
55. Harms, A. S. *et al.* Peripheral monocyte entry is required for alpha-Synuclein induced inflammation and Neurodegeneration in a model of Parkinson disease. *Exp. Neurol.* **300,** 179–187 (2018).
56. Brochard, V. *et al.* Infiltration of CD4+ lymphocytes into the brain contributes to neurodegeneration in a mouse model of Parkinson disease. *J. Clin. Invest.* **119,** 182–192 (2009).
57. Schetters, S. T. T., Gomez-Nicola, D., Garcia-Vallejo, J. J. & Van Kooyk, Y. Neuroinflammation: Microglia and T Cells Get Ready to Tango. *Front. Immunol.* **8,** 547–11 (2018).
58. Lindestam Arlehamn, C. S., Garretti, F., Sulzer, D. & Sette, A. Roles for the adaptive immune system in Parkinson's and Alzheimer's diseases. *Curr Opin Immunol* **59,** 115–120 (2019).
59. Reynolds, A. D., Stone, D. K., Mosley, R. L. & Gendelman, H. E. Nitrated α-Synuclein-Induced Alterations in Microglial Immunity Are Regulated by CD4+ T Cell Subsets. *J Immunol* **182,** 4137–4149 (2009).
60. Reynolds, A. D., Stone, D. K., Mosley, R. L. & Gendelman, H. E. Proteomic Studies of Nitrated Alpha-Synuclein Microglia Regulation by CD4+CD25+ T Cells. *J Proteome Res* **8,** 3497–3511 (2009).
61. Duffy, M. F. *et al.* Lewy body-like alpha-synuclein inclusions trigger reactive microgliosis prior to nigral degeneration. *J Neuroinflam* **15**, 129 (2018).
62. Grabert, K. *et al.* Microglial brain region–dependent diversity and selective regional sensitivities to aging. *Nat Neurosci* **19,** 504–516 (2016).
63. Lawson, L. J., Perry, V. H., Dri, P. & Gordon, S. Heterogeneity in the distribution and morphology of microglia in the normal adult mouse brain. *Neuroscience* **39,** 151–170 (1990).
64. Geirsdottir, L. *et al.* Cross-Species Single-Cell Analysis Reveals Divergence of the Primate Microglia Program. *Cell* **179,** 1609–1622.e16 (2019).
65. Mihara, T. *et al.* Natural killer cells of Parkinson's disease patients are set up for activation: A possible role for innate immunity in the pathogenesis of this disease. *Parkinsonism & Related Disorders* **14,** 46–51 (2008).
66. Caligiuri, M. A. Human natural killer cells. *Blood* **112,** 461–469 (2008).
67. Hao, J. *et al.* Central nervous system (CNS)–resident natural killer cells suppress Th17 responses and CNS autoimmune pathology. *J. Exp. Med.* **207,** 1907–1921 (2010).
68. Earls, R. H. *et al.* NK cells clear α-synuclein and the depletion of NK cells exacerbates synuclein pathology in a mouse model of α-synucleinopathy. *Proc Natl Acad Sci* **117,** 1762-1771 (2020).
69. Marsden, M. D. & Zack, J. A. Humanized Mouse Models for Human Immunodeficiency Virus Infection. *Annu. Rev. Virol.* **4,** 393–412 (2017).
70. Clark, E. A. & Ledbetter, J. A. How B and T cells talk to each other. *Nature* **367,** 425–428 (1994).

Figure 1

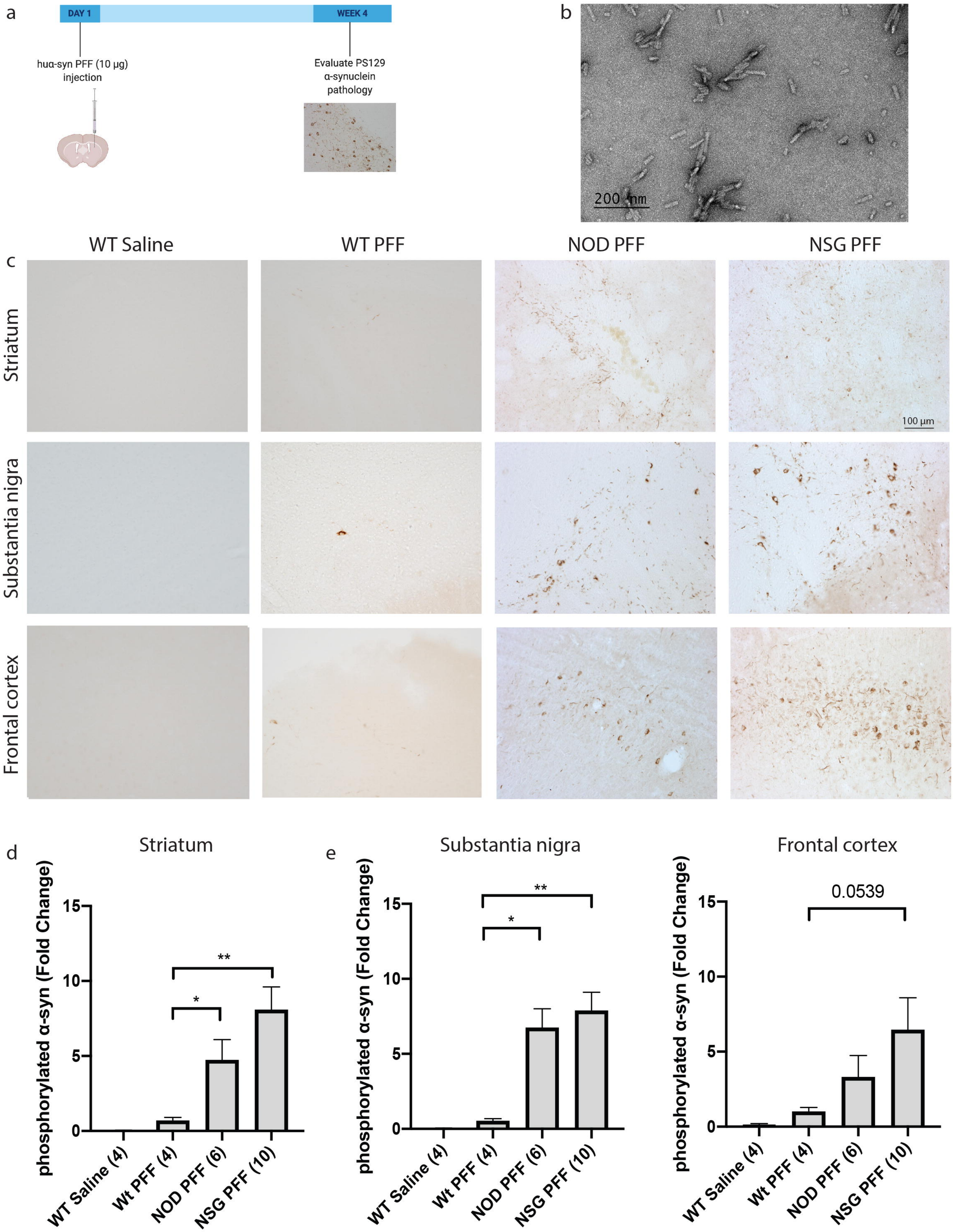
a
DAY 1
WEEK 4
huα-syn PFF (10 μg) injection
Evaluate PS129 α-synuclein pathology
b
200 nm
WT Saline
WT PFF
NOD PFF
NSG PFF
c
Striatum
Substantia nigra
Frontal cortex
100 μm
d
Striatum
phosphorylated α-syn (Fold Change)
15
10
5
0
**
*
WT Saline (4)
Wt PFF (4)
NOD PFF (6)
NSG PFF (10)
e
Substantia nigra
phosphorylated α-syn (Fold Change)
15
10
5
0
**
*
WT Saline (4)
Wt PFF (4)
NOD PFF (6)
NSG PFF (10)
Frontal cortex
phosphorylated α-syn (Fold Change)
15
10
5
0
0.0539
WT Saline (4)
Wt PFF (4)
NOD PFF (6)
NSG PFF (10)

Figure 2

a

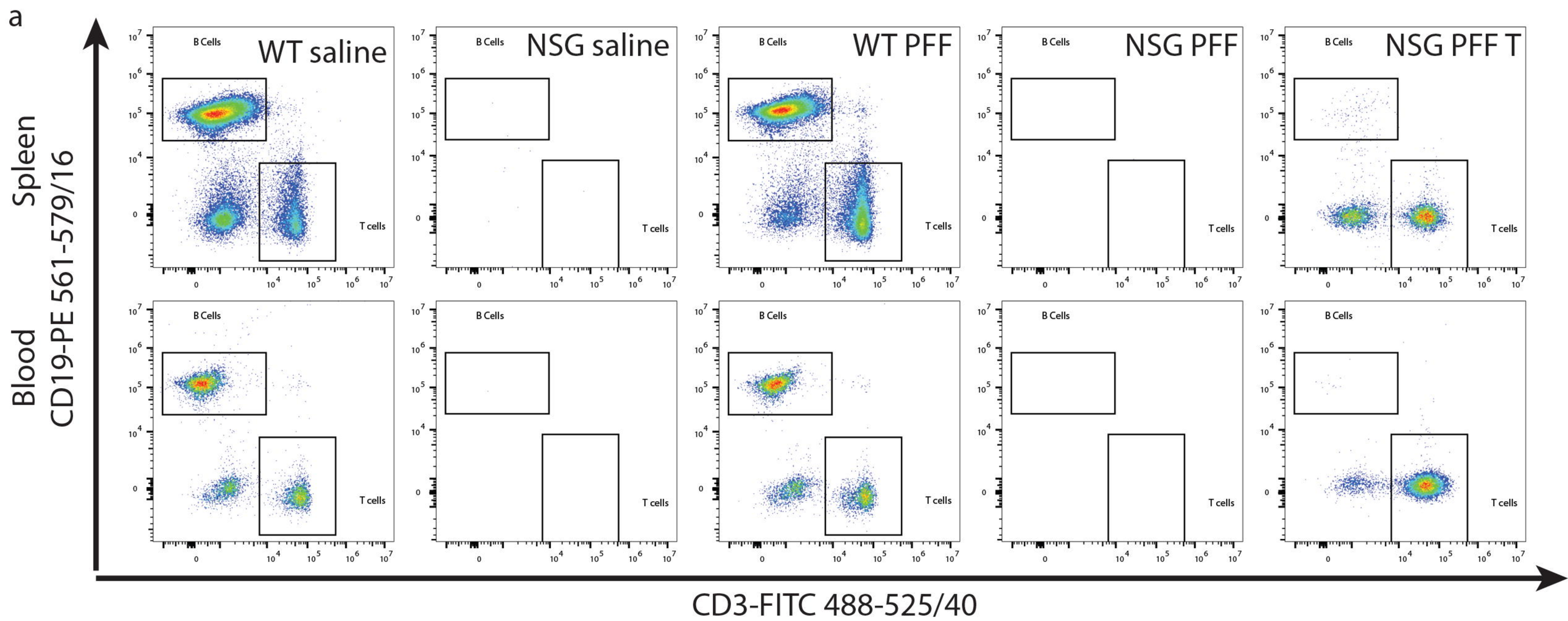
WT saline
NSG saline
WT PFF
NSG PFF
NSG PFF T
B Cells
T cells
Spleen
Blood
CD19-PE 561-579/16
CD3-FITC 488-525/40

b

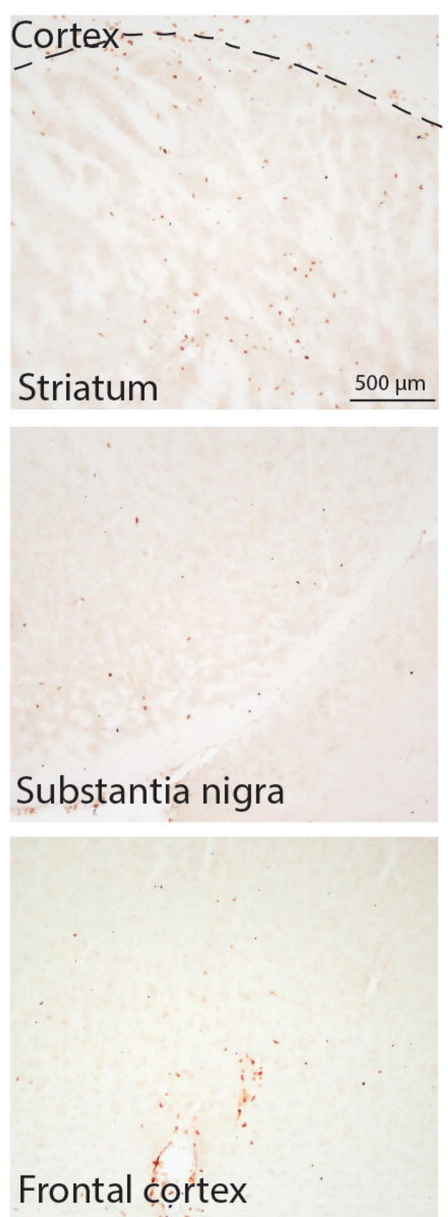
CD3
Cortex
Striatum
500 µm
Substantia nigra
Frontal cortex

c

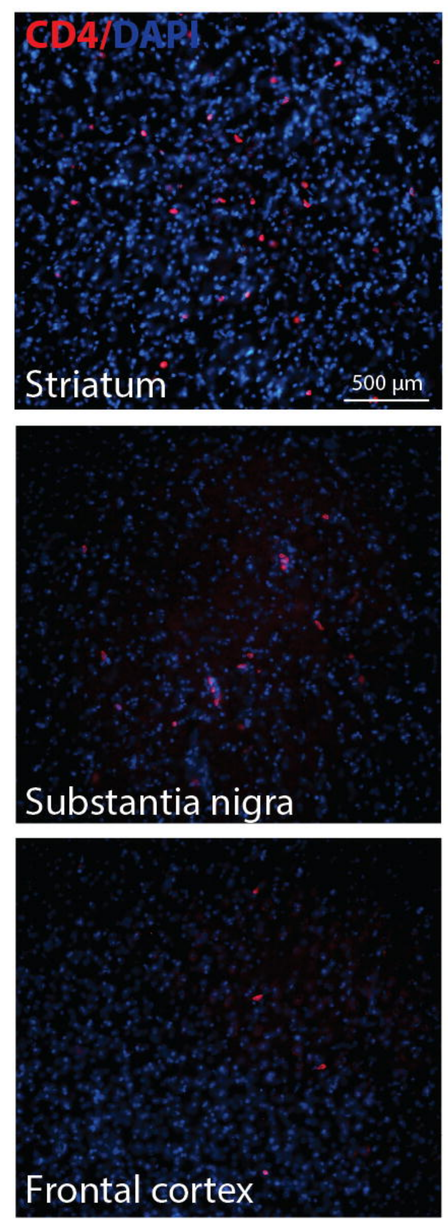
CD4/DAPI
Striatum
500 µm
Substantia nigra
Frontal cortex

Figure 3

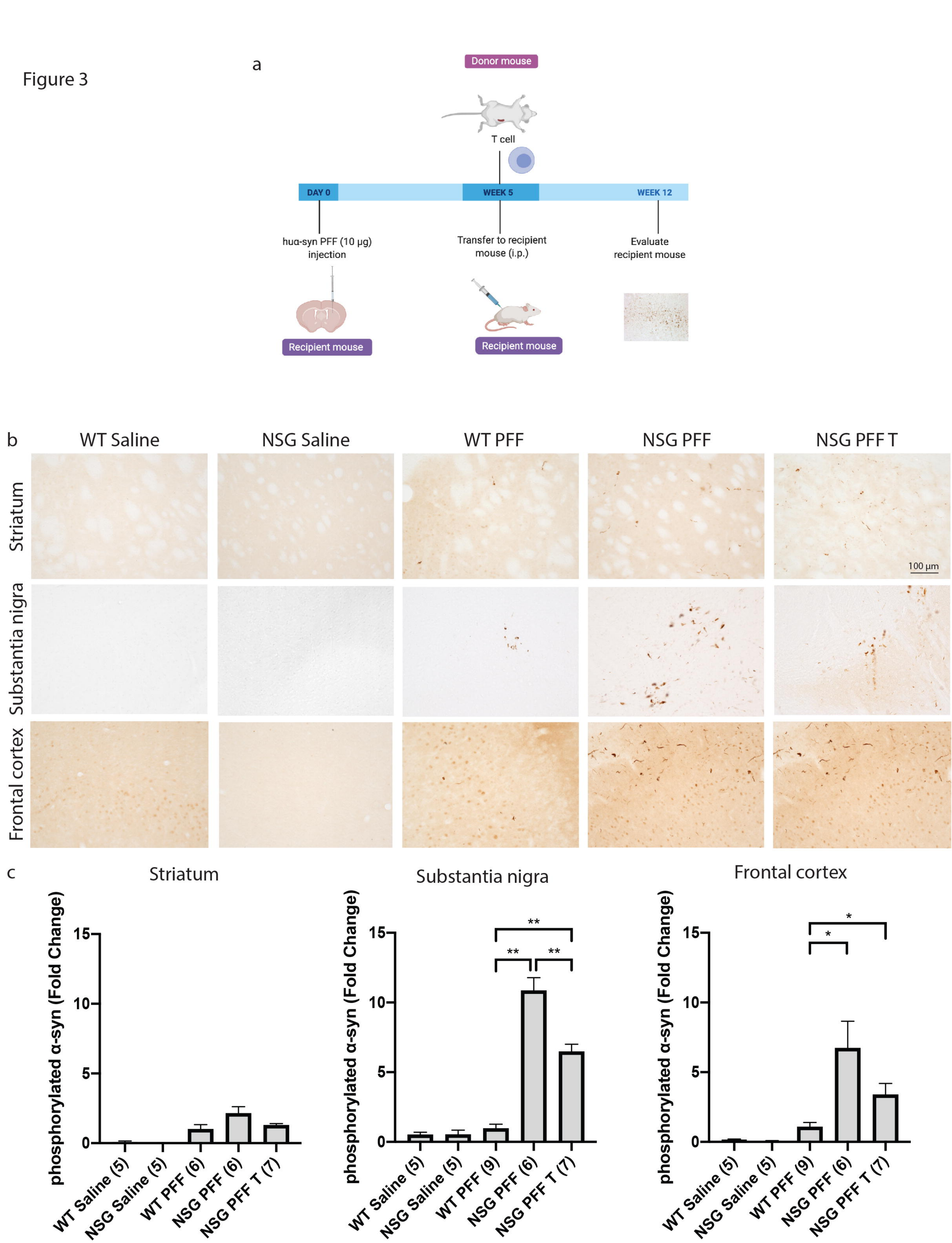
a
Donor mouse
T cell
DAY 0
WEEK 5
WEEK 12
huα-syn PFF (10 μg) injection
Transfer to recipient mouse (i.p.)
Evaluate recipient mouse
Recipient mouse
Recipient mouse
b
WT Saline
NSG Saline
WT PFF
NSG PFF
NSG PFF T
Striatum
Substantia nigra
Frontal cortex
100 μm
c
Striatum
Substantia nigra
Frontal cortex
phosphorylated α-syn (Fold Change)
15
10
5
0
WT Saline (5)
NSG Saline (5)
WT PFF (6)
NSG PFF (6)
NSG PFF T (7)
WT PFF (9)
**
*

Figure 4

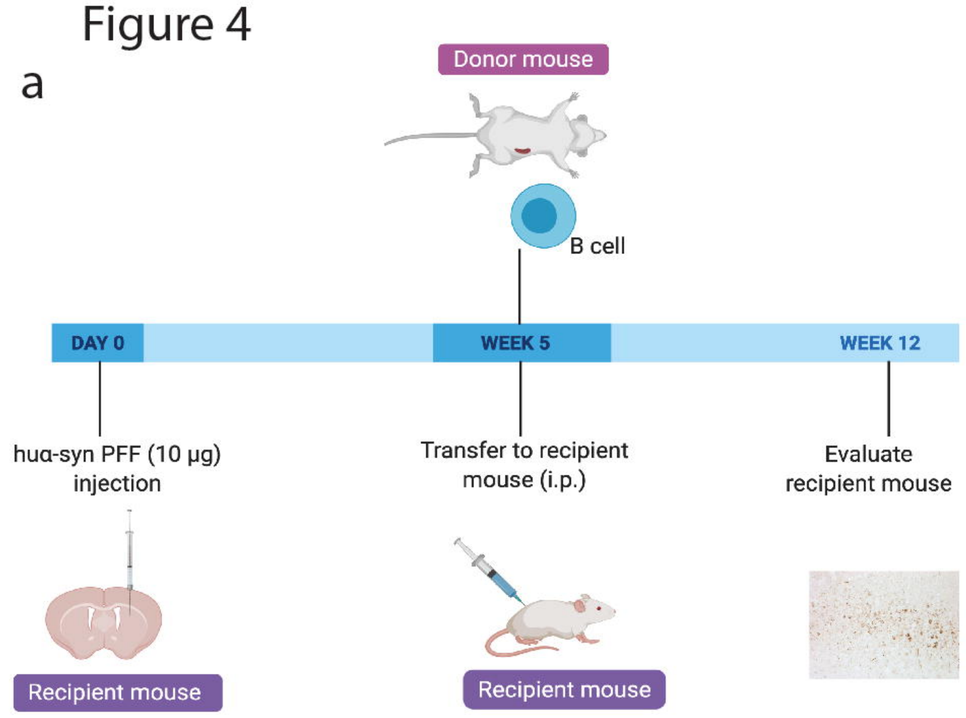
a
Donor mouse
B cell
DAY 0
WEEK 5
WEEK 12
huα-syn PFF (10 μg) injection
Transfer to recipient mouse (i.p.)
Evaluate recipient mouse
Recipient mouse
Recipient mouse

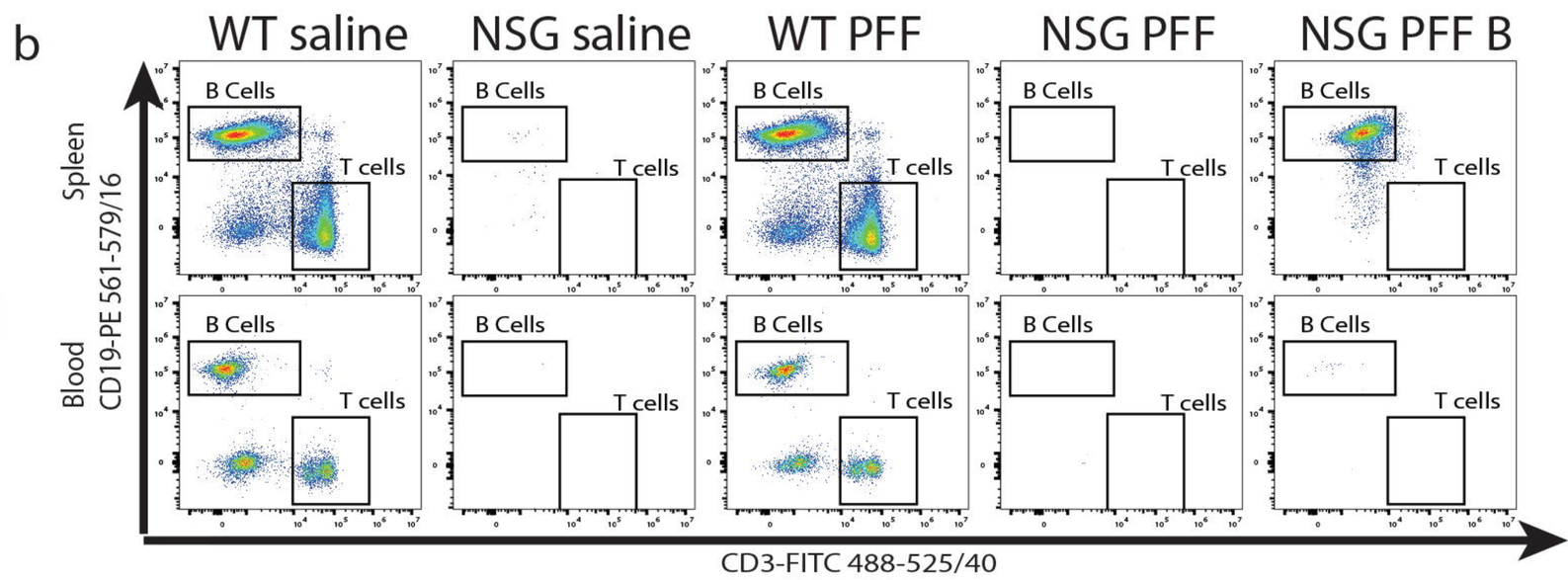
b
WT saline
NSG saline
WT PFF
NSG PFF
NSG PFF B
Spleen
Blood
CD19-PE 561-579/16
CD3-FITC 488-525/40
B Cells
T cells

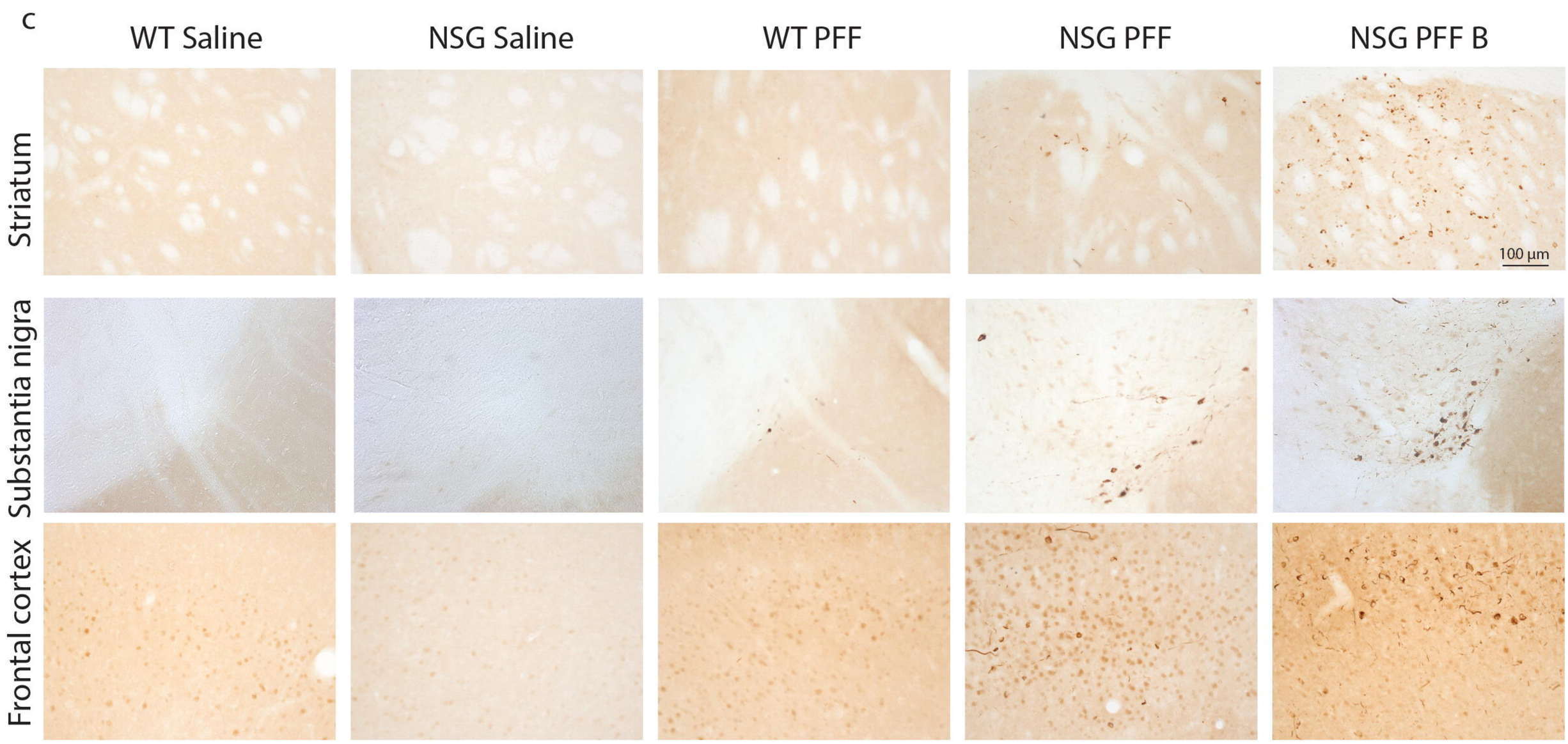
c
WT Saline
NSG Saline
WT PFF
NSG PFF
NSG PFF B
Striatum
Substantia nigra
Frontal cortex
100 μm

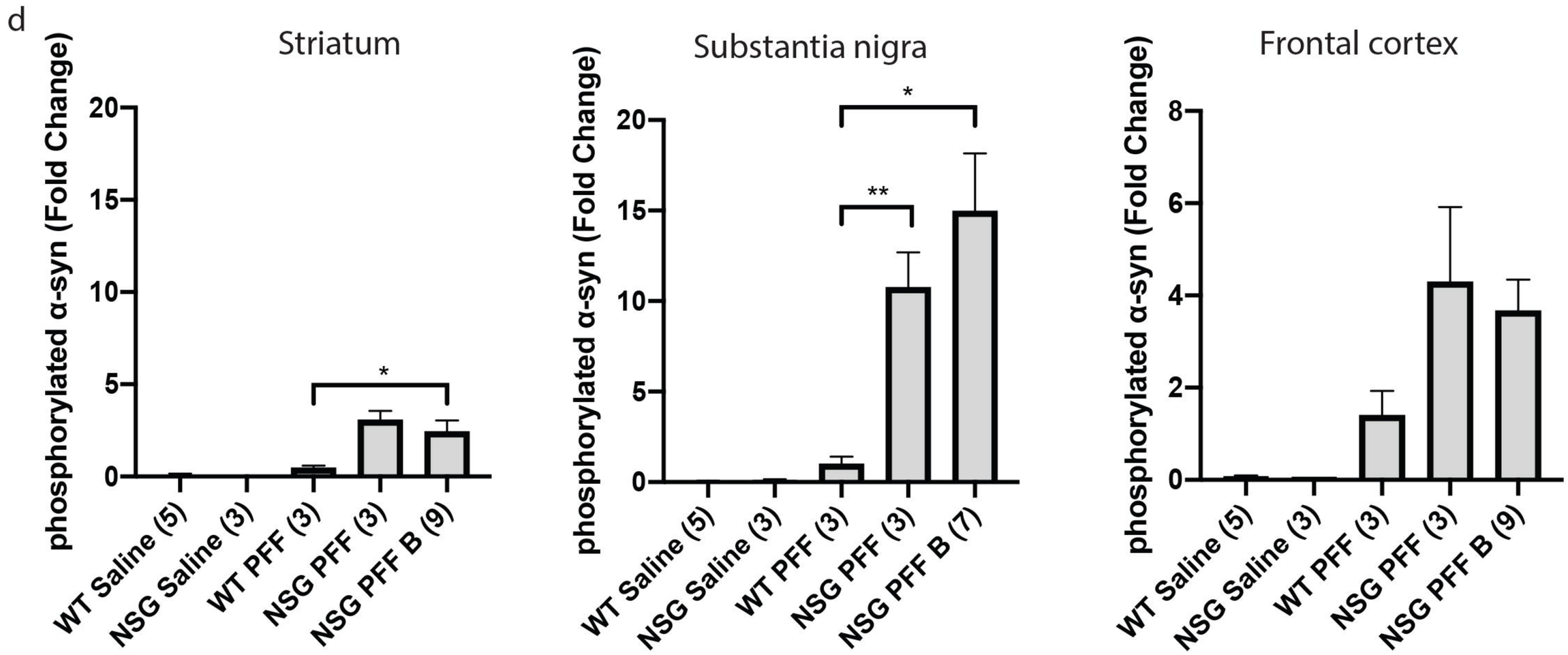
d
Striatum
Substantia nigra
Frontal cortex
phosphorylated α-syn (Fold Change)
WT Saline (5)
NSG Saline (3)
WT PFF (3)
NSG PFF (3)
NSG PFF B (9)
NSG PFF B (7)
*
**

Figure 5

a

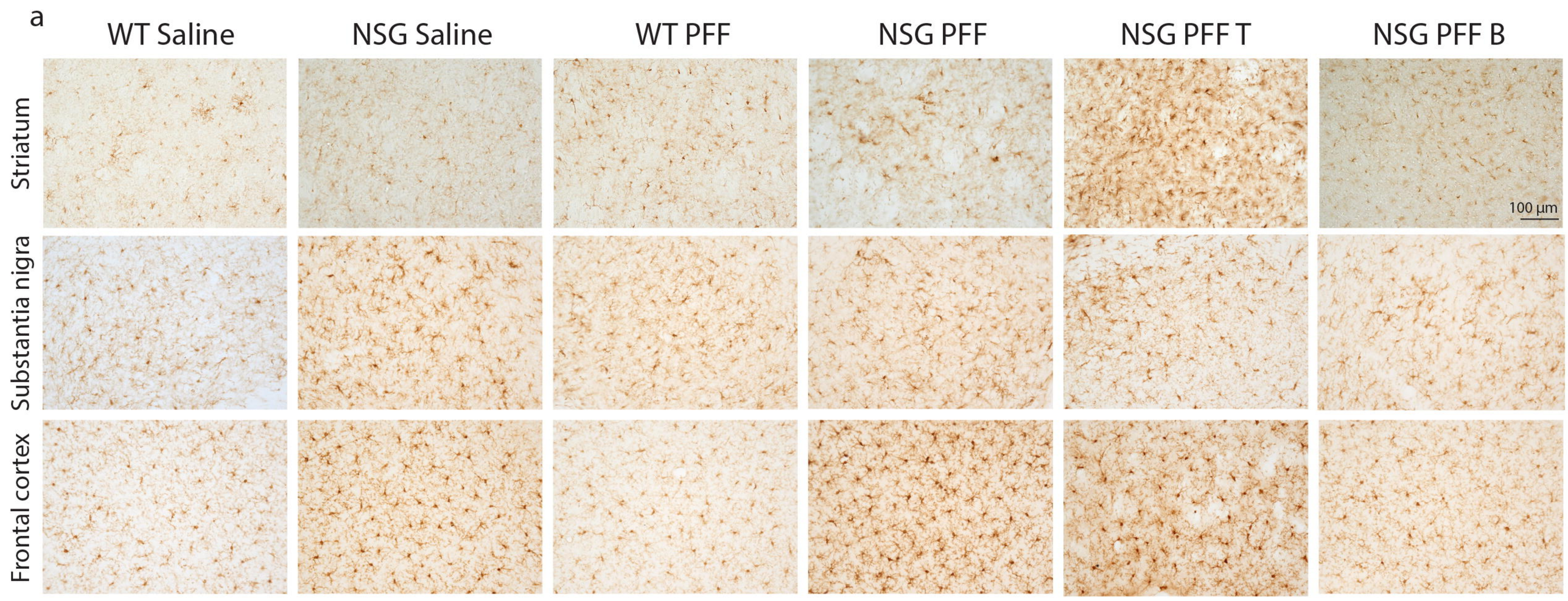

b

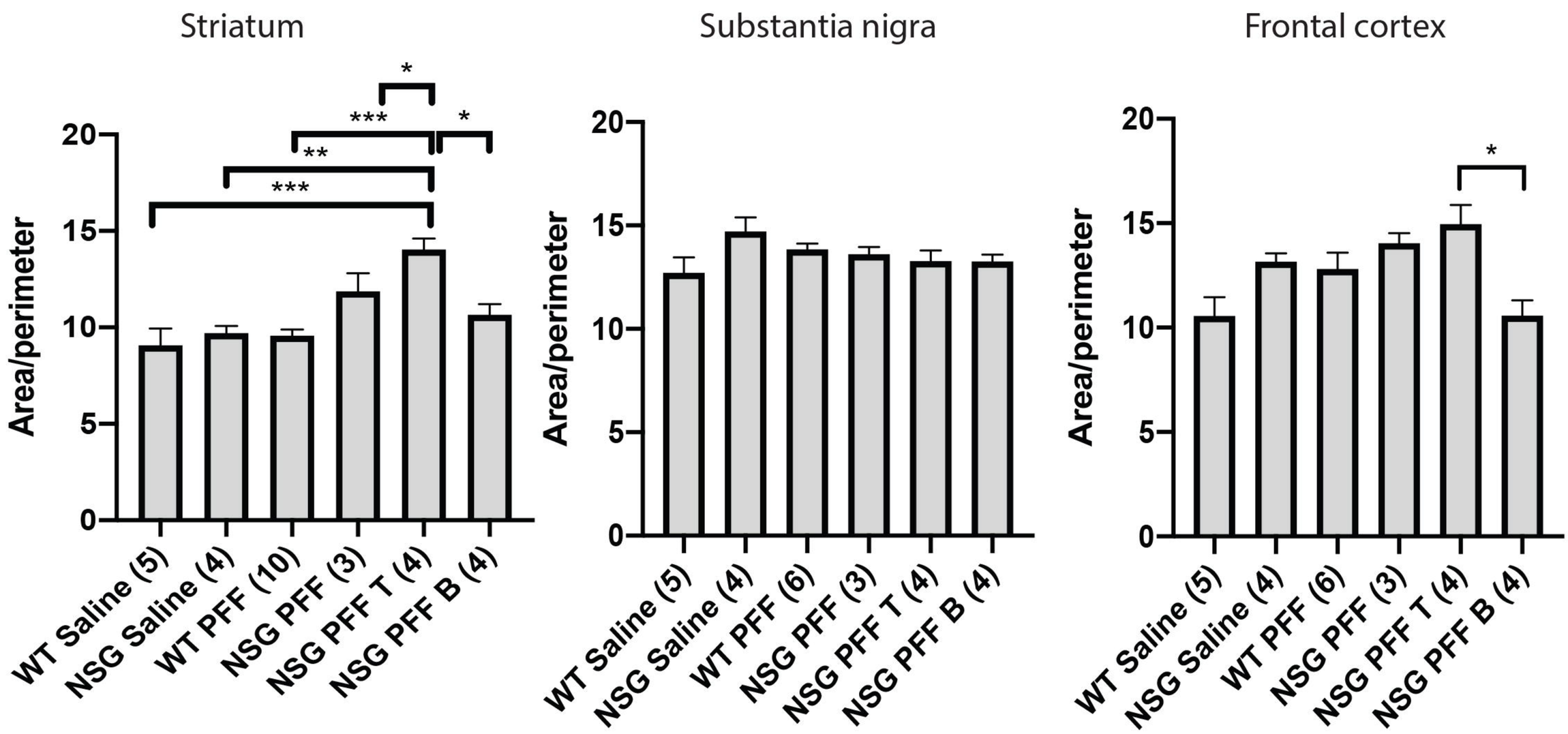

c

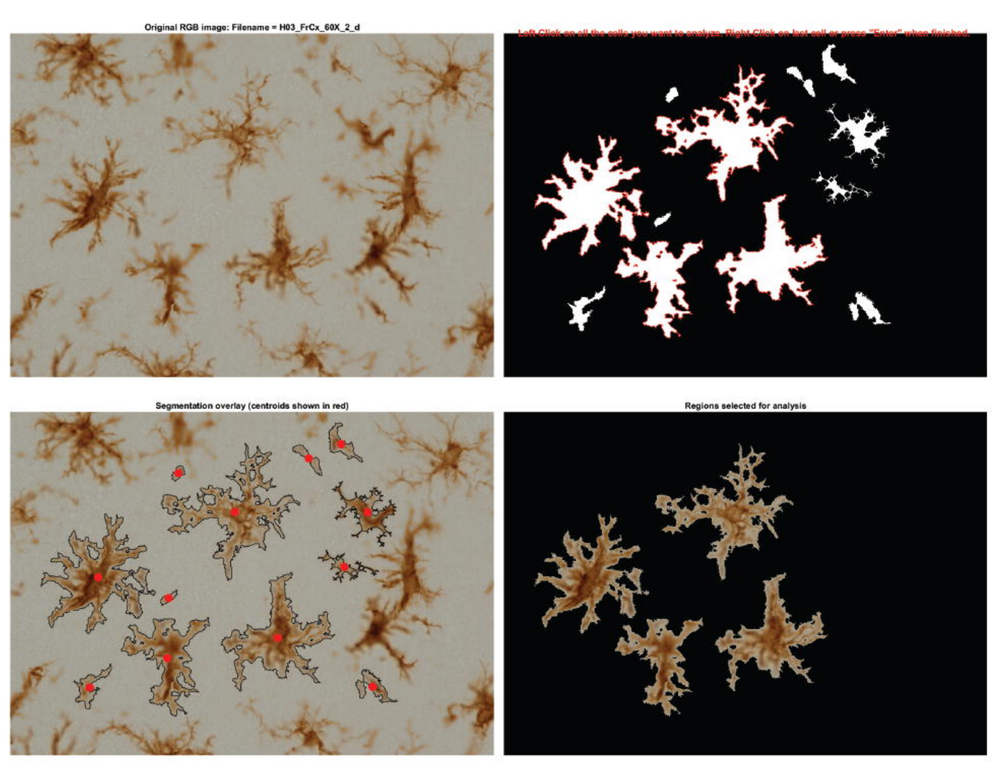
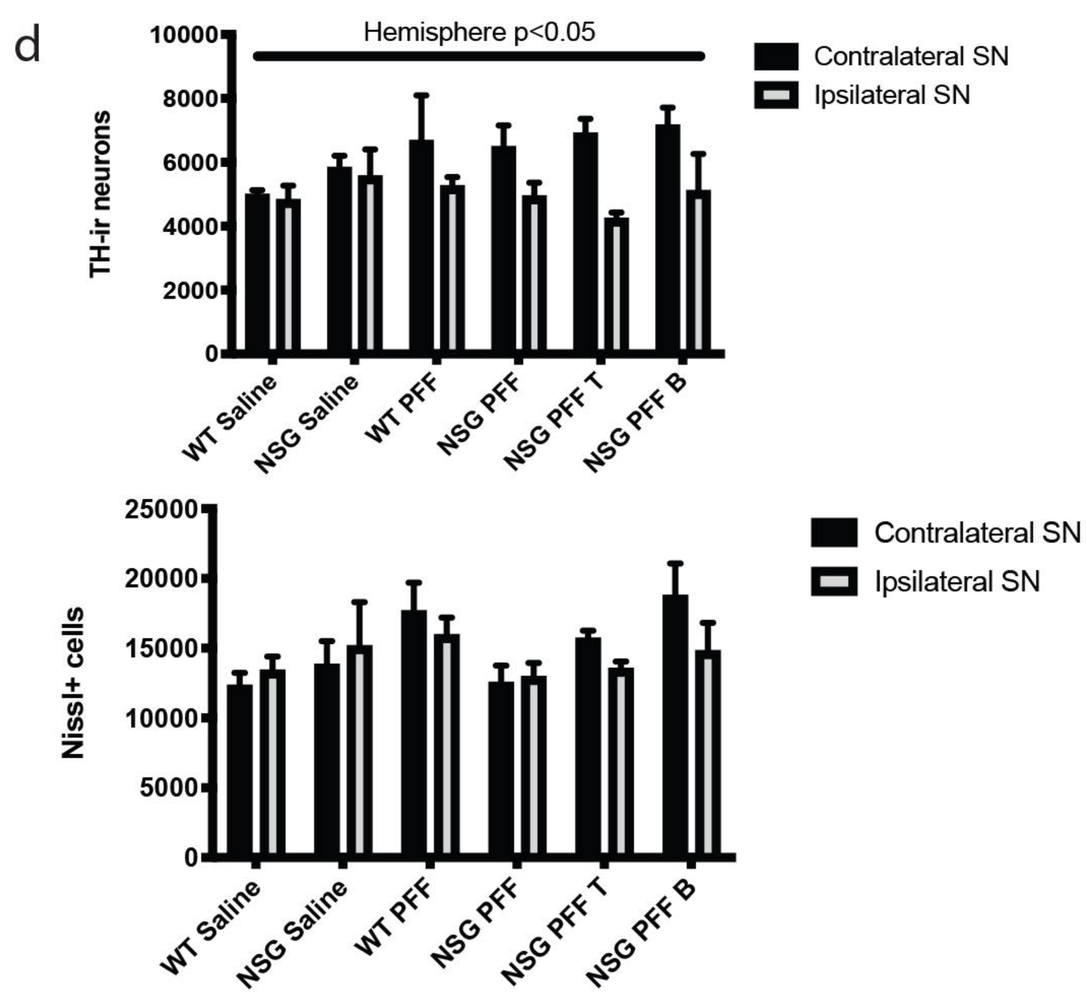
d